

Image Guided Cost Aggregation for Hierarchical Depth Map Fusion

Thilo Borgmann and Thomas Sikora

Communication Systems Group, Technische Universität Berlin, Berlin, Germany

Keywords: Multi View Stereo, Stereo Matching, Depth Estimation, Depth Map Fusion.

Abstract: Estimating depth from a video sequence is still a challenging task in computer vision with numerous applications. Like other authors we utilize two major concepts developed in this field to achieve that task which are the hierarchical estimation of depth within an image pyramid as well as the fusion of depth maps from different views. We compare the application of various local matching methods within such a combined approach and can show the relative performance of local image guided methods in contrast to commonly used fixed-window aggregation. Since efficient implementations of these image guided methods exist and the available hardware is rapidly enhanced, the disadvantage of their more complex but also parallel computation vanishes and they will become feasible for more applications.

1 INTRODUCTION

Reconstructing a three-dimensional representation of a scene from multiple images of a video sequence is one of the most important topics in computer vision. It serves as an essential basis for numerous application from different areas like robotics, medical imaging, video processing and many more. Intense research on this topic has been done for many years and the state-of-the-art advances rapidly. Yet it is still a challenging task to acquire high-quality 3D reconstructions using image-based methods only.

The enormous amount of algorithms proposed to accomplish this task use a wide variety of approaches. The most important property to distinguish between these algorithms is their scope of matching and optimization, either locally or globally. This categorization holds in general, even though there are some approaches in between. Algorithms utilizing a global optimization tend to produce the most accurate results. Unfortunately, achieving this quality usually requires complex computations and is therefore not always feasible with respect to the desired application. Also, these algorithms usually provide limited capabilities of parallelization. Thus even modern computer hardware cannot compensate this drawback due to their still limited computation of sequential parts of these algorithms.

In contrast to these methods, algorithms based on local matching approaches are much less complex and offer the advantage of rapid computation. Although

they usually suffer from the ambiguities within their local scope. Early approaches show a severe difference in quality compared to their globally optimized counterparts. However, recent improvements to local matching can significantly reduce the gap between the two categories. Always considering a limited local area only, these methods also offer excellent possibilities for parallelization. Modern computer hardware in turn provide a basis for such massive parallel computation so that the number of high-quality real-time capable algorithms permanently increase.

For a comprehensive overview of existing methods and their relative performance evaluation, we refer to the publicly available benchmarks covering this topic (Scharstein et al., 2001) (Seitz et al., 2006) (Strecha et al., 2008).

Nevertheless, there is always the trade-off between quality and computational complexity. Given a set of calibrated images from a video sequence, we utilize two major concepts developed in this area, which are the hierarchical estimation of depth maps (Yang and Pollefeys, 2003) (Zach et al., 2004) (Cornelis and Van Gool, 2005) (Nalpantidis et al., 2009) and the fusion of depth maps from multiple views (Zitnick et al., 2004) (Merrell et al., 2007) (Zach, 2008) (Zhang et al., 2009) (Unger et al., 2010).

The fusion of the depth maps allows to achieve a high quality while the hierarchical structure of the depth estimation helps to reduce complexity. We are not the first to combine these approaches (McKinnon et al., 2012). The authors evaluated the influence of

several parameters to their approach but the choice of the initial depth map estimation and cost aggregation is just roughly covered. The several authors of the former contributions about hierarchical estimation and depth map fusion do also not report comparatively about different estimation approaches. Thus, in contrast to other methods, our contribution is to reveal the relative performance of the applied cost aggregation used throughout the hierarchical estimation process instead of focusing on a sophisticated processing on or between the higher levels of the approach. Although a global matching algorithm seems feasible at that stage of the hierarchical processing, the relative overhead remains and we stick to local methods. We therefore implemented and compared the performance of several well-known cost aggregation methods that have already been proven their ability to achieve high-quality estimation results as well as being computational efficient. We integrate them into a rather simple hierarchical scheme for the applied cost aggregation to be the dominant factor within this process. This leads us to the relative performance of the initial depth map and cost aggregation used in such a hierarchical framework.

2 RELATED WORK

Common two-view disparity estimation algorithms compute separate disparity maps for each of the two views, postprocessed by a left-right consistency check. By applying that, ambiguous matches and occluded pixels are detected. This approach has also been transferred and adapted for depth estimation in multi-view matching (Zitnick et al., 2004) (Merrell et al., 2007).

Hierarchical disparity matching is also a common approach in the field of stereo matching. In (Yang and Pollefeys, 2003) (Zach et al., 2004) (Cornelis and Van Gool, 2005) the authors successfully demonstrate the real-time capabilities and efficiency of their approaches.

A combination of the former methods is presented in (McKinnon et al., 2012). The authors describe an iterative approach of the fusion of depth maps throughout their hierarchical estimation scheme. Within each level of the hierarchy, the depth map is further refined by an iterative application of the connectivity constraint (Cornelis and Van Gool, 2005).

Many cost aggregation methods have been proposed based on variable support regions (Tombari et al., 2008a). Among many that dynamically select different or multiple support windows (Hirschmüller

et al., 2002) or varying window sizes (Veksler, 2003), we concentrate on those approaches that define the support region based on the local surrounding within the image like (Yoon and Kweon, 2006) (Tombari et al., 2008b) (Zhang et al., 2009) (He et al., 2010). We refer to these as image guided aggregation methods.

Cost aggregation methods are amongst the most important things to consider for stereo matching algorithms. According to the rapid development of these algorithms, cost aggregation methods are also rapidly enhanced. Next to benchmarks like (Scharstein et al., 2001) (Strecha et al., 2008), which evaluate complete algorithms, the bare cost initialization and aggregation methods have also been addressed by other contributions.

In (Wang et al., 2006) the authors evaluate a set of well-known cost initialization methods in combination with image guided and unguided cost aggregations. They use several sequences from the Middlebury stereo data set to compare the resulting disparity estimations. All methods are evaluated by being incorporated into the same disparity estimator. Concerning the evaluated image guided cost aggregation methods they approve the expected gain in quality of the disparity estimation. They also show the increasing complexity when using these methods.

A very comprehensive evaluation of cost initializations and cost aggregations as well as their relation to each other has been done in (Tombari et al., 2008a). Many different image guided aggregation methods have been evaluated also using the Middlebury stereo data set. They use a simplistic winner-takes-all approach to generate their results for a clear dependency on the incorporated initialization and aggregation methods. We instead do not only cover the quality of the generated depth map but also the influence of repeatedly applied depth map fusion and refinement using the corresponding cost and aggregation methods.

3 HIERARCHICAL ALGORITHM

For our hierarchical implementation, we adopt several techniques from previous approaches of (Cornelis and Van Gool, 2005) and (McKinnon et al., 2012).

We iterate through an image pyramid. Each level k of the pyramid holds frames of half the width and height of the size of the succeeding level. In this implementation, we reduce the resolution for the lowest level of the pyramid to $1 / 64$ th of the full resolution. Due to our hardware limitations, we have to restrict the highest level of the pyramid to $1 / 4$ th of the full

resolution (1536x1024 pixels).

For the first level $k = 0$ of this hierarchy, we apply an initial plane-sweep based estimation. For each succeeding level $k > 0$, we apply a refining depth map based sweep adopted from (Cornelis and Van Gool, 2005). The depth estimates of the current level are then processed by a depth map fusion before the algorithm proceeds to the next level in the hierarchy. For that, all depth estimates of the current level have to be concurrently computed. After the first level $k = 0$ has been processed, the parameters r_k and d_k that influence the refining depth map sweep used in all levels $k > 0$ are updated according to the current level. This hierarchical approach can be seen as a simplified variant of the scheme presented in (McKinnon et al., 2012) with just one refinement iteration within the levels of the hierarchy.

The following pseudo code outlines the described algorithm:

```

For all levels k
  For all cameras
    If k = 0 then
      Initial Depth Estimation
    Else
       $r_k = k * r_0$ 
       $d_k = 1/2 * d_{k-1}$ 
      Depth Map Sweep
    Fi
  Depth Map Fusion
End
End

```

In the following sections we briefly outline each individual step and describe the influence of the parameters r_k and d_k .

3.1 Initial Depth Estimation

For each camera, we basically apply a fronto-parallel plane-sweep approach (Collins, 1996). We divide the sequence into two halves for the preceding and succeeding views according to (Kang et al., 2001). The number of views projected onto the sweep-plane might vary, but we found using one view to be sufficient. The sweep-plane is then projected into the reference camera and for each depth the photo-consistency function according to the applied cost and aggregation methods is computed.

Throughout all depths we apply a simple winner-takes-all approach to receive the minimal cost for each pixel. A simple parabolic interpolation is applied using the depth and cost values of the sweep-layers in front and behind the minimum plane to achieve a continuous depth value.

A second sweep follows with the projecting view used as the reference view to apply a standard

left-right consistency check to remove ambiguous matches. This bidirectional sweeping procedure is applied using the preceding as well as the succeeding views. The combination of both intermediate depth maps $D_{i,L}$, $D_{i,R}$ results in a continuous depth map for each reference view $D_i = D_{i,L} \cup D_{i,R}$. Note that one of these bidirectional sweeps can be reused for the depth map estimation of the succeeding reference view: $D_{i-1,R} = D_{i,L}$. Thus, for each camera pair of the sequence just one bidirectional sweep has to be computed. The initial depth estimation is followed by the first depth map fusion that is equal to all levels.

3.2 Depth Map Sweep

The fused depth maps from the previous level $k - 1$ are swept again using the current resolution within a small range d_k around the current depth estimate (Cornelis and Van Gool, 2005). This range around the estimate is decreased to half the size of the previous level:

$$d_k = \frac{1}{2} d_{k-1} \quad (1)$$

The respective window or kernel sizes s depend on a given parameter r_k , so that $s = (2r_k + 1)^2$. For the cross-based method of (Zhang et al., 2009), r_k defines the maximum arm length used. The value of r_k is linearly increased by the current level on basis of the initial size:

$$r_k = k r_0 \quad (2)$$

For the image guided aggregation methods, a second parameter e is required that controls the image guided creation of the support region. This parameter is fixed for all applications of the corresponding aggregation but differs according to the method used. However, for our simplified hierarchical approach we rely on the refined sampling interval and the enforced smoothness during the fusion stage to enhance the estimation and do not incorporate a connectivity constraint.

3.3 Depth Map Fusion

In this stage the depth maps of the surrounding views generated in the same level are projected into the reference view. We apply only two simple validations to reject outliers from being candidates for the fusion.

First, we accept only candidates that are within a close distance ϵ to the reference estimation and therefore support its location (Merrell et al., 2007). Second, the euclidean distance between the color vectors of the reference pixel and the candidate pixel is tested to be within another threshold θ . From the set of remaining candidates, we apply another winner-takes-

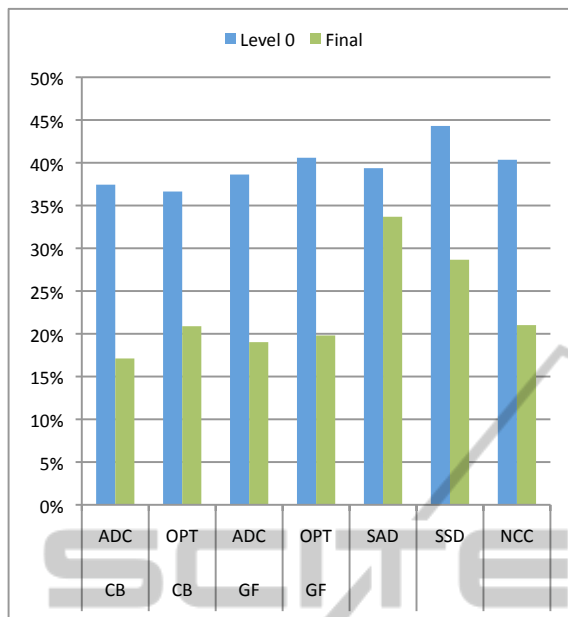


Figure 1: Comparison of the fusion results of all combinations using their respective best performing parameters for ‘Fountain’.

all approach to select the candidate with the smallest cost value corresponding to its origin view.

The last step is to apply a mean filter to smooth the fused depth maps. To preserve depth discontinuities, we compute this filter within a cross-based support region generated by (Zhang et al., 2009) using a small maximum arm length r_f . The used parameters θ , ϵ and r_f are constant for all levels. The fused depth maps are then passed to the next iteration on the succeeding level.

4 EVALUATION

We compare several approaches for cost initialization and cost aggregation used to compute the photo-consistency function during the plane-sweeps.

Some of the most common combinations are the absolute intensity differences and the squared intensity differences, aggregated within a fixed-window to form the well-known sum of absolute differences (SAD) and sum of squared differences (SSD) cost functions. Next to these, there is also the normalized cross-correlation (NCC) to be considered in this category.

For the comparison with image guided cost functions, we have chosen two state-of-the-art approaches. The first is the guided image filtering (GF) approach presented in (He et al., 2010). The second is the cross-based aggregation method (CB) of (Zhang

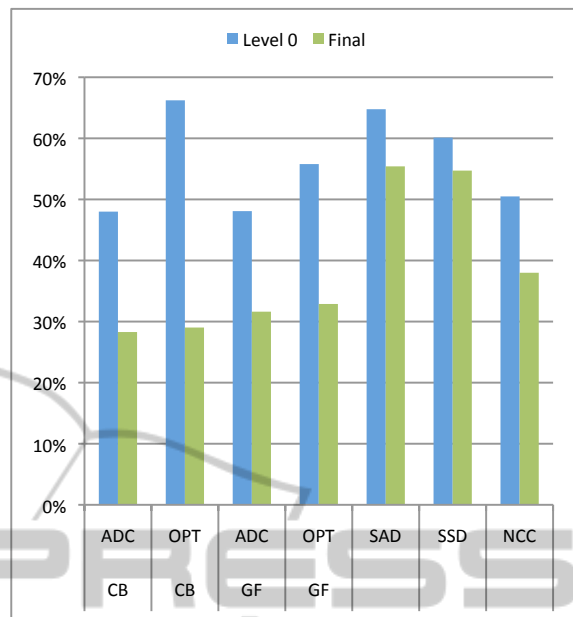


Figure 2: Comparison of the fusion results of all combinations using their respective best performing parameters for ‘Herz-Jesu’.

et al., 2009). Among many alternatives to these aggregation methods, these two have proven to perform very accurately in state-of-the-art stereo matching algorithms (Rhemann et al., 2011) (Mei et al., 2011) and also provide very efficient implementations using integral images (Crow, 1984). In (Mei et al., 2011) the cross-based aggregation is applied to a cost initialization based on a linear combination of the absolute differences and the census transform called AD-Census (ADC). In (Rhemann et al., 2011) a common cost initialization based on the absolute differences and gradients (OPT) is used, well-known from many contributions concerning the optical flow computation.

Therefore we include in our comparison both these combinations (CB + ADC, GF + OPT) as well as the combination of exchanged initialization and aggregation methods (CB + OPT, GF + ADC). Thus, we have a set of seven combinations to be evaluated in our hierarchical framework.

We have chosen two well-known wide-baseline outdoor sequences from the data set provided by (Strecha et al., 2008) for our evaluation: ‘Fountain’ and ‘Herz-Jesu’. These sequences feature a ground-truth 3D-model, acquired using a laser range scanner, and ground-truth camera calibration. We measure the quality of our results by projecting the ground-truth model into all processed cameras of the sequence. For each pixel the resulting depth value of that projection is then compared to the depth values generated by our hierarchical algorithm. We generate a histogram of

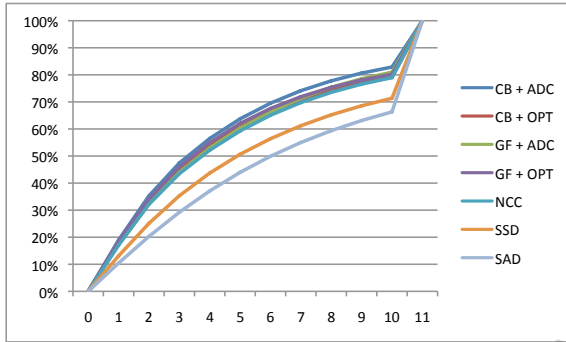


Figure 3: Cumulative distribution of best performing combinations for sequence ‘Fountain’.

eleven bins to accumulate pixels according to their depth difference. Like (McKinnon et al., 2012), we define a threshold σ equivalent to 3mm for each bin of the histogram. All estimates with a difference greater than 10σ as well as all missing pixels according to the ground-truth are accumulated in the last bin. This histogram is closely related to the evaluation scheme used in (Strecha et al., 2008) and (McKinnon et al., 2012). It reveals the precision of the estimated pixels as well as the completeness in terms of the given threshold of 10σ .

We compare the various combinations of cost and aggregation methods primarily by their amount of precisely estimated pixels. For that we can utilize the last bin of the histogram. The lower that value the more pixels have been estimated with a sufficient precision and the better the aggregation method performs. The values presented are given by percentage of all pixels estimated. In figure 1 and figure 2 we compare the best performing parameters for all seven combinations applied to the according sequence. For each combination, the result after the first depth map fusion at level $k = 0$ and the result of the final depth map fusion are shown. This illustrates the overall performance as well as the benefits of the hierarchical processing. The corresponding parameters are given in table 1. In figure 3 and figure 4 we show the according cumulative distribution to visualize the relative precision for these combinations, too. For the best and worst performing image guided and fixed methods, we show the color-coded differences to the ground-truth for a subimage of both sequences in figure 5. The pixel-wise differences are color-coded according to bins of the corresponding histogram, from white for small differences less or equal to σ to black for differences up to 10σ . All blue pixels represent differences of more than 10σ .

We use the parameters given in table 2 for the complete evaluation. The parameters r_0 and e influence the behavior of the aggregation methods and

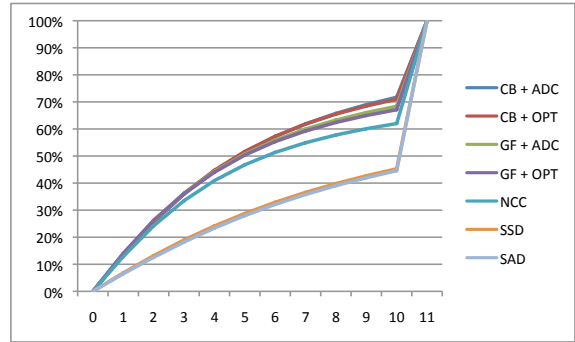


Figure 4: Cumulative distribution of best performing combinations for sequence ‘Herz-Jesu’.

Table 1: Best performing parameter values for each combination and sequence.

Agg.	Cost	e	r_0	Level 0	Final
Fountain:					
CB	ADC	12	3	37,4383	17,1133
CB	OPT	12	3	36,6367	20,8848
GF	ADC	0,001	1	38,6234	19,0225
GF	OPT	0,001	2	40,5867	19,8058
	SAD		1	39,3672	33,6869
	SSD		2	44,3056	28,6606
	NCC		2	40,3505	21,0151
Herz-Jesu:					
CB	ADC	5	1	48,0009	28,2878
CB	OPT	5	2	66,2230	29,0251
GF	ADC	0,100	1	48,0823	31,6208
GF	OPT	0,100	1	55,7852	32,8818
	SAD		1	64,7667	55,4109
	SSD		2	60,1193	54,7170
	NCC		1	50,4895	37,9934

Table 2: Parameter values used for the parameter-sweep.

Parameter	Value(s)
θ	0.2
r_f	r_0
d_1	0.3
ϵ	0.1
r_0	1, 2, 3, 4, 6
$e(GF)$	0.1, 0.01, 0.001
$e(CB)$	5, 8, 12

are therefore assigned several values for a parameter-sweep. Note that e depends on the image guided method and has completely different values assigned. For the guided image filter (He et al., 2010), this value is similar to ϵ of the original implementation. For the cross-based aggregation (Zhang et al., 2009), this value corresponds to τ .

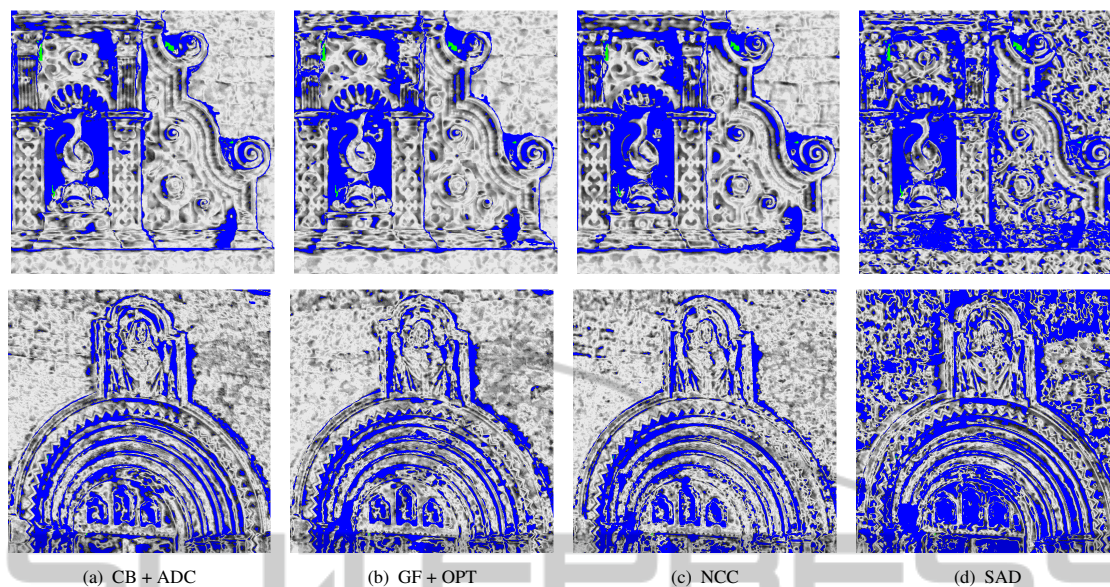


Figure 5: Subimages of both sequences showing the pixel-wise evaluation by color-coded differences to the ground-truth. Differences range from $\leq 1\sigma$ (white) to $\leq 10\sigma$ (black). Blue color indicates a difference of $> 10\sigma$. Sequence ‘Fountain’ is shown in the upper row, sequence ‘Herz-Jesu’ is shown in the lower row. The best (a) and the worst (b) image guided combinations as well as the best (c) and the worst (d) fixed methods are shown.

5 CONCLUSIONS

We can show in our evaluation that the application of image guided methods generally produce a more complete and precise result, see figures 1, 2, 3, 4 and 5. For the ‘Fountain’ sequence, the difference between the best performing image guided and non-guided method is around 4%, and almost 10% for ‘Herz-Jesu’. Although the normalized cross-correlation performs almost as well as the image guided approach (GF + OPT) on the ‘Fountain’ sequence, the difference becomes larger in a more complex sequence like ‘Herz-Jesu’. Nevertheless, it clearly outperforms the SAD and SSD approaches on both sequences.

Thus, the application of image guided methods has its benefits although they require a slightly more complex computation. However, this disadvantage vanishes due to the improving hardware capabilities in terms of parallel computing. The normalized cross-correlation offers a good trade-off between quality and complexity for both sequences. These results encourage us to further investigate the application of image guided methods in a more sophisticated hierarchical estimation approach.

ACKNOWLEDGEMENTS

The authors like to thank David M^cKinnon, Ryan Smith and Ben Upcroft for their most valuable support of various data and personal contact.

REFERENCES

- Collins, R. (1996). A space-sweep approach to true multi-image matching. In *Computer Vision and Pattern Recognition, 1996. Proceedings CVPR’96, 1996 IEEE Computer Society Conference on*, pages 358–363. IEEE.
- Cornelis, N. and Van Gool, L. (2005). Real-time connectivity constrained depth map computation using programmable graphics hardware. In *Computer Vision and Pattern Recognition, 2005. CVPR 2005. IEEE Computer Society Conference on*, volume 1, pages 1099–1104. IEEE.
- Crow, F. (1984). Summed-area tables for texture mapping. *ACM SIGGRAPH Computer Graphics*, 18(3):207–212.
- He, K., Sun, J., and Tang, X. (2010). Guided image filtering. *Computer Vision—ECCV 2010*, pages 1–14.
- Hirschmüller, H., Innocent, P., and Garibaldi, J. (2002). Real-time correlation-based stereo vision with reduced border errors. *International Journal of Computer Vision*, 47(1):229–246.
- Kang, S., Szeliski, R., and Chai, J. (2001). Handling occlusions in dense multi-view stereo. In *Computer Vision*

- and Pattern Recognition, 2001. *CVPR 2001. Proceedings of the 2001 IEEE Computer Society Conference on*, volume 1, pages 1–103. IEEE.
- McKinnon, D., Smith, R., and Upcroft, B. (2012). A semi-local method for iterative depth-map refinement. In *Proceedings of the IEEE International Conference on Robotics and Automation (ICRA 2012)*. IEEE.
- Mei, X., Sun, X., Zhou, M., Jiao, S., Wang, H., and Zhang, X. (2011). On building an accurate stereo matching system on graphics hardware. In *Computer Vision Workshops (ICCV Workshops), 2011 IEEE International Conference on*, pages 467–474. IEEE.
- Merrell, P., Akbarzadeh, A., Wang, L., Mordohai, P., Frahm, J., Yang, R., Nistér, D., and Pollefeys, M. (2007). Real-time visibility-based fusion of depth maps. In *Computer Vision, 2007. ICCV 2007. IEEE 11th International Conference on*, pages 1–8. IEEE.
- Nalpantidis, L., Amanatiadis, A., Sirakoulis, G., Kyriakoulis, N., and Gasteratos, A. (2009). Dense disparity estimation using a hierarchical matching technique from uncalibrated stereo vision. In *Imaging Systems and Techniques, 2009. IST '09. IEEE International Workshop on*, pages 427–431.
- Rhemann, C., Hosni, A., Bleyer, M., Rother, C., and Gelautz, M. (2011). Fast cost-volume filtering for visual correspondence and beyond. In *Computer Vision and Pattern Recognition (CVPR), 2011 IEEE Conference on*, pages 3017–3024. IEEE.
- Scharstein, D., Szeliski, R., and Zabih, R. (2001). A taxonomy and evaluation of dense two-frame stereo correspondence algorithms. In *Stereo and Multi-Baseline Vision, 2001. (SMBV 2001). Proceedings. IEEE Workshop on*, pages 131–140.
- Seitz, S., Curless, B., Diebel, J., Scharstein, D., and Szeliski, R. (2006). A comparison and evaluation of multi-view stereo reconstruction algorithms. In *Computer Vision and Pattern Recognition, 2006 IEEE Computer Society Conference on*, volume 1, pages 519–528.
- Strecha, C., von Hansen, W., Van Gool, L., Fua, P., and Thoennessen, U. (2008). On benchmarking camera calibration and multi-view stereo for high resolution imagery. In *Computer Vision and Pattern Recognition, 2008. CVPR 2008. IEEE Conference on*, pages 1–8.
- Tombari, F., Mattocchia, S., Di Stefano, L., and Addimanda, E. (2008a). Classification and evaluation of cost aggregation methods for stereo correspondence. In *Computer Vision and Pattern Recognition, 2008. CVPR 2008. IEEE Conference on*, pages 1–8. IEEE.
- Tombari, F., Mattocchia, S., Di Stefano, L., and Addimanda, E. (2008b). Near real-time stereo based on effective cost aggregation. In *Pattern Recognition, 2008. ICPR 2008. 19th International Conference on*, pages 1–4. IEEE.
- Unger, C., Wahl, E., Sturm, P., Ilic, S., et al. (2010). Probabilistic disparity fusion for real-time motion-stereo. Citeseer.
- Veksler, O. (2003). Fast variable window for stereo correspondence using integral images. In *Computer Vision and Pattern Recognition, 2003. Proceedings. 2003 IEEE Computer Society Conference on*, volume 1, pages 1–556. IEEE.
- Wang, L., Gong, M., Gong, M., and Yang, R. (2006). How far can we go with local optimization in real-time stereo matching. In *3D Data Processing, Visualization, and Transmission, Third International Symposium on*, pages 129–136. IEEE.
- Yang, R. and Pollefeys, M. (2003). Multi-resolution real-time stereo on commodity graphics hardware. In *Computer Vision and Pattern Recognition, 2003. Proceedings. 2003 IEEE Computer Society Conference on*, volume 1, pages 1–211. IEEE.
- Yoon, K. and Kweon, I. (2006). Adaptive support-weight approach for correspondence search. *Pattern Analysis and Machine Intelligence, IEEE Transactions on*, 28(4):650–656.
- Zach, C. (2008). Fast and high quality fusion of depth maps. In *Proceedings of the International Symposium on 3D Data Processing, Visualization and Transmission (3DPVT)*, volume 1.
- Zach, C., Karner, K., and Bischof, H. (2004). Hierarchical disparity estimation with programmable 3d hardware. In *Proc. of WSCG, Pilsen, Czech Republic*, pages 275–282.
- Zhang, G., Jia, J., Wong, T., and Bao, H. (2009). Consistent depth maps recovery from a video sequence. *Pattern Analysis and Machine Intelligence, IEEE Transactions on*, 31(6):974–988.
- Zitnick, C., Kang, S., Uyttendaele, M., Winder, S., and Szeliski, R. (2004). High-quality video view interpolation using a layered representation. In *ACM Transactions on Graphics (TOG)*, volume 23, pages 600–608. ACM.

APPENDIX

The complete evaluation data is given in separate tables. There are two tables for each sequence, one for fixed-window and one for image guided aggregation, respectively. Tables 3 and 5 show the results for the sequence ‘Fountain’ and tables 4 and 6 show the results for the sequence ‘Herz-Jesu’. The values given in the columns ‘Level 0’ and ‘Final’ are the percentages of pixels estimated with an insufficient precision after the first and final depth map fusion, respectively.

Table 3: Parameter-sweep of image guided aggregation for the 'Fountain' sequence.

Agg.	Cost	e	r_0	Level 0	Final
CB	ADC	5	1	37,7922	21,3303
CB	ADC	5	2	39,6136	20,5099
CB	ADC	5	3	38,6625	19,3956
CB	ADC	5	4	39,418	19,5801
CB	ADC	5	6	39,617	17,6259
CB	ADC	8	1	37,6795	21,4545
CB	ADC	8	2	39,5631	19,9244
CB	ADC	8	3	38,295	18,7349
CB	ADC	8	4	39,2334	17,7528
CB	ADC	8	6	40,1979	18,2764
CB	ADC	12	1	37,4367	18,4192
CB	ADC	12	2	39,2775	17,5535
CB	ADC	12	3	37,4383	17,1133
CB	ADC	12	4	39,6574	18,3329
CB	ADC	12	6	41,2455	19,3537
CB	OPT	5	1	40,0748	25,8658
CB	OPT	5	2	38,81	22,9363
CB	OPT	5	3	37,6746	21,7772
CB	OPT	5	4	38,2792	22,32
CB	OPT	5	6	38,0735	20,92
CB	OPT	8	1	40,7023	25,9492
CB	OPT	8	2	38,2409	21,7358
CB	OPT	8	3	37,1505	21,1068
CB	OPT	8	4	37,797	21,4484
CB	OPT	8	6	39,1751	20,9398
CB	OPT	12	1	41,4982	25,3186
CB	OPT	12	2	37,9567	21,3778
CB	OPT	12	3	36,6367	20,8848
CB	OPT	12	4	38,15	21,4235
CB	OPT	12	6	40,157	21,5007
GF	ADC	0,100	1	40,3396	19,2574
GF	ADC	0,100	2	41,895	21,2373
GF	ADC	0,100	3	43,4714	24,6391
GF	ADC	0,100	4	45,3187	27,7024
GF	ADC	0,100	6	49,313	34,1429
GF	ADC	0,010	1	39,8775	19,0698
GF	ADC	0,010	2	41,4333	20,5663
GF	ADC	0,010	3	42,659	23,2175
GF	ADC	0,010	4	44,3367	25,9867
GF	ADC	0,010	6	48,1713	31,8384
GF	ADC	0,001	1	38,6234	19,0225
GF	ADC	0,001	2	40,3896	19,2996
GF	ADC	0,001	3	41,9276	21,7289
GF	ADC	0,001	4	43,5808	24,1429
GF	ADC	0,001	6	46,6741	28,7754
GF	OPT	0,100	1	38,567	19,9531
GF	OPT	0,100	2	43,6802	20,5242
GF	OPT	0,100	3	45,5161	32,7966
GF	OPT	0,100	4	47,1033	26,9157
GF	OPT	0,100	6	50,8852	33,962
GF	OPT	0,010	1	38,2503	20,3005
GF	OPT	0,010	2	43,0723	20,2045
GF	OPT	0,010	3	44,9116	22,2674
GF	OPT	0,010	4	46,2428	25,172
GF	OPT	0,010	6	49,1156	31,8687
GF	OPT	0,001	1	38,4306	21,452
GF	OPT	0,001	2	40,5867	19,8058
GF	OPT	0,001	3	43,3264	20,8162
GF	OPT	0,001	4	44,8305	23,0555
GF	OPT	0,001	6	47,3774	28,2155

Table 4: Parameter-sweep of image guided aggregation for the 'Herz-Jesu' sequence.

Agg.	Cost	e	r_0	Level 0	Final
CB	ADC	5	1	48,0009	28,2878
CB	ADC	5	2	47,3767	28,2884
CB	ADC	5	3	46,8367	28,5651
CB	ADC	5	4	47,3276	28,7136
CB	ADC	5	6	47,5468	28,5672
CB	ADC	8	1	48,1184	29,9848
CB	ADC	8	2	47,3707	29,2522
CB	ADC	8	3	46,6911	29,4477
CB	ADC	8	4	47,5492	29,4454
CB	ADC	8	6	48,1225	29,5938
CB	ADC	12	1	48,4898	30,3152
CB	ADC	12	2	47,2583	29,5847
CB	ADC	12	3	46,8833	29,7205
CB	ADC	12	4	47,9632	30,0588
CB	ADC	12	6	48,9818	30,7885
CB	OPT	5	1	71,747	29,2853
CB	OPT	5	2	66,223	29,0251
CB	OPT	5	3	64,3264	29,3956
CB	OPT	5	4	65,0884	29,6815
CB	OPT	5	6	60,622	29,4952
CB	OPT	8	1	73,0595	35,323
CB	OPT	8	2	64,381	34,3963
CB	OPT	8	3	62,5112	34,4801
CB	OPT	8	4	62,9131	34,3226
CB	OPT	8	6	58,353	29,7987
CB	OPT	12	1	74,7221	35,5511
CB	OPT	12	2	62,9915	34,6381
CB	OPT	12	3	59,9426	34,7855
CB	OPT	12	4	61,5115	34,746
CB	OPT	12	6	57,2033	30,474
GF	ADC	0,100	1	48,0823	31,6208
GF	ADC	0,100	2	51,1138	33,5118
GF	ADC	0,100	3	54,2877	36,0289
GF	ADC	0,100	4	57,3762	38,4606
GF	ADC	0,100	6	62,8878	40,9152
GF	ADC	0,010	1	48,2435	32,5278
GF	ADC	0,010	2	50,6403	33,9099
GF	ADC	0,010	3	53,485	36,1495
GF	ADC	0,010	4	56,2268	38,1879
GF	ADC	0,010	6	61,3152	40,5947
GF	ADC	0,001	1	48,3742	33,0063
GF	ADC	0,001	2	49,9871	33,9849
GF	ADC	0,001	3	52,6447	36,0113
GF	ADC	0,001	4	55,4582	37,9339
GF	ADC	0,001	6	60,3802	40,1883
GF	OPT	0,100	1	55,7852	32,8818
GF	OPT	0,100	2	53,0231	34,265
GF	OPT	0,100	3	55,9169	36,6067
GF	OPT	0,100	4	59,4258	38,9416
GF	OPT	0,100	6	64,8294	41,5739
GF	OPT	0,010	1	58,5235	33,8893
GF	OPT	0,010	2	53,3666	34,6742
GF	OPT	0,010	3	55,0431	36,8447
GF	OPT	0,010	4	58,0632	38,7642
GF	OPT	0,010	6	63,1551	40,9723
GF	OPT	0,001	1	64,0341	34,0826
GF	OPT	0,001	2	53,9388	34,7354
GF	OPT	0,001	3	54,3004	36,3368
GF	OPT	0,001	4	56,6877	38,252
GF	OPT	0,001	6	61,6086	40,4988

Table 5: Parameter-sweep of fixed-window aggregation for the 'Fountain' sequence.

Cost	r_0	Level 0	Final
SAD	1	39,3672	33,6869
SAD	2	44,57	33,7516
SAD	3	48,4126	35,219
SAD	4	51,3834	36,9954
SAD	6	57,1401	42,3865
SSD	1	39,407	31,9276
SSD	2	44,3056	28,6606
SSD	3	47,9115	31,4935
SSD	4	51,4584	36,0764
SSD	6	57,7117	43,349
NCC	1	37,5055	23,2568
NCC	2	40,3505	21,0151
NCC	3	43,9219	26,8657
NCC	4	47,4144	32,4665
NCC	6	55,3231	41,7527

Table 6: Parameter-sweep of fixed-window aggregation for the 'Herz-Jesu' sequence.

Cost	r_0	Level 0	Final
SAD	1	64,7667	55,4109
SAD	2	62,3676	57,3074
SAD	3	64,4764	58,7674
SAD	4	67,3589	60,8153
SAD	6	73,2592	63,8015
SSD	1	62,4588	55,9535
SSD	2	60,1193	54,717
SSD	3	63,1757	56,7857
SSD	4	67,0811	59,2385
SSD	6	73,7221	63,2108
NCC	1	50,4895	37,9934
NCC	2	45,292	41,0395
NCC	3	53,5491	44,9542
NCC	4	61,095	49,067
NCC	6	70,8198	53,7205